Experimental analysis and practical effectiveness correlations of enthalpy wheels

Stefano De Antonellis*, Manuel Intini, Cesare Maria Joppolo, Federico Pedranzini

Dipartimento di Energia, Politecnico di Milano, Via Lambruschini, 4, 20156 Milan, Italy

Received 4 April 2014
Received in revised form 30 July 2014
Accepted 1 August 2014
Available online 11 August 2014

1. Introduction

It is well known that buildings are responsible for around 40% of primary energy consumption in developed countries and for 20–40% in developing countries [1]. In the construction of new buildings or in case of refurbishment of existing ones, the use of heat exchangers between exhaust and fresh air streams can provide relevant energy savings, reducing both heating and cooling load [2,3]. In particular, interest in enthalpy wheels is increasing due to sensible and latent heat recovery capability, low pressure drops and high effectiveness.

An enthalpy wheel consists of a cylindrical rotating device made of rolled-up corrugated sheets of metallic material (such as aluminium), in order to get a great number of parallel channels with a typical sinusoidal or triangular cross sectional geometry (Fig. 1). The metallic substrate is coated with a sorption material, such as silica gel, activated alumina, molecular sieve or calcium carbonate, which is able to adsorb water vapour. Two air streams pass through the cross section area of the device: typically the outside fresh air stream, referred to as supply air, and the exhaust one, which is the return air flow from the building. A purge sector between exhaust and process air streams can be used to reduce contamination of the fresh air flow.

* Corresponding author. Tel.: +39 0223993823; fax: +39 0223993913.
E-mail address: stefano.deantonellis@polimi.it (S. De Antonellis).

Heat and moisture are transferred from the former air stream to the wheel matrix and then from the matrix to the latter air stream. For a given enthalpy wheel, operating parameters such as revolution speed, supply and exhaust air temperature, humidity and velocity, influence the behaviour of the component.

When energy analysis of buildings and HVAC systems is carried out, enthalpy wheel performance should be properly evaluated. A simplified approach is often used in literature: sensible and latent effectiveness are assumed constant or are determined by linear interpolation of values at different air flows [4,5]. In spite of its simplicity, it may lead to improper performance evaluation because these terms are not constant over a wide range of working conditions. For this reason several works are available in literature in order to properly predict the behaviour of enthalpy wheels.

Many detailed models have been developed, solving heat and mass transfer equations [6–10]. This approach is particularly suitable to design enthalpy wheels and analyse its performance, but it requires high calculation time because a system of partial differential equations should be solved. Although studies to simplify the set of governing equations have been already proposed [11–14], correlation based approach would be certainly more suitable for energy simulation tools since it is faster and more effective than the previous one.

Rabah et al. [15] tested a commercial sensible heat wheel, with supply air temperature ranging from 40 °C to 70 °C, providing effectiveness correlations based on Kays and London [16] equations. These working conditions are interesting for desiccant evaporative

Nomenclature

a_c	channel height [mm]
A	area [m^2]
$A, B \ldots N$	test set
b_c	channel base [mm]
D	diameter [m]
cp	moist air specific heat [$J\,kg^{-1}\,K^{-1}$]
$C_{1,2\ldots10}$	correlation parameters
$D_{1,2}$	duct
$EW1$	enthalpy wheel no. 1
$EW2$	enthalpy wheel no. 2
L	enthalpy wheel length [m]
$\dot{m}$	mass flow rate [$kg\,s^{-1}$]
$n_{1,2,3}$	correlation exponents [−]
N	revolution speed [$rev\,min^{-1}$]
NTU	number of transfer units [−]
p	pressure [Pa]
$\dot{Q}$	heat transfer rate [W]
R	ratio between the minimum and maximum inlet air velocity times air density [−]
T	temperature [°C]
UA	overall heat transfer conductance times surface area [$W\,K^{-1}$]
u_ε	effectiveness uncertainty [−]
u_{xi}	uncertainty of a generic measured parameter [°C, Pa or %]
$u_{xi,inst}$	instrument uncertainty of a generic measured parameter [°C, Pa or %]
v	face velocity [$m\,s^{-1}$]
x_i	generic measured parameter [°C, Pa or %]
X	humidity ratio [$kg_v\,kg_{da}{}^{-1}$]

Greek symbols

α, β	effectiveness correction terms [−]
φ	relative humidity [%]
Δp	pressure drop [Pa]
ε	effectiveness [−]
λ	water latent heat of vaporization [$J\,kg^{-1}$]
ρ	density [$kg\,m^{-3}$]
ν	cinematic viscosity [$m^2\,s^{-1}$]

Subscripts

a	air
ave	average
d	distributed pressure drop
EW	enthalpy wheel
ea	exhaust air
h	hub
in	inlet
l	local pressure drop
L	latent
o	outer
op	orifice plate
out	outlet
S	sensible
sa	supply air
tot	total
$vsat$	saturated water vapour

cooling cycles but they do not represent typical inlet air conditions of heat exchangers for energy recovery in buildings.

Several authors [17–19] provided simplified effectiveness correlations of enthalpy wheels, obtained from numerical results of detailed component models, instead of directly from experimental data. Stiesch [17] proposed sensible and total effectiveness correlations as a function of temperature, number of transfer units, and dimensionless revolution speed, considering balanced flows and constant exhaust air temperature. Simonson and Besant [18] developed complex correlations of sensible and latent effectiveness, in particular they considered the effect of the adsorption isotherm, the ratio of latent to sensible heat exchanged, the average temperature and the average relative humidity. Finally Jeong and Mumma [19] developed effectiveness correlations as a function of inlet air temperature, relative humidity, and face velocity, providing two equations that require several coefficients.

All in all there is a lack of correlations that can be easily adopted in yearly basis energy simulation tools, in order to predict sensible and latent effectiveness and pressure drop of enthalpy wheels. In this work two different enthalpy wheels, that represent the state of the art in the field, are experimentally tested and practical equations to predict their performance are proposed.

2. Experimental methodology

2.1. Experimental setup

The facility is designed to provide two air streams at accurate controlled conditions of temperature, humidity and flow. The two air streams, denoted as the supply air and the exhaust air, feed the enthalpy wheel in a counter current arrangement. A schematic representation of the experimental setup is shown in Fig. 2.

Temperature and humidity are properly controlled through heating coils, cooling coils and evaporative coolers, in order to reach most typical working conditions of enthalpy wheels in HVAC systems. The supply air stream unit is equipped with additional electrical heaters to adjust flow temperature up to 120 °C (in recirculation mode) for desiccant wheels tests. The enthalpy wheel casing is divided in four equal partitions in each side. Each stream enters and leaves the wheel through two partitions connected with two parallel flexible ducts. Temperature and relative humidity of each air stream are measured at the inlet (in one point) and outlet (in two points) of the wheel through sensors located in the cross section of the duct. As reported in Fig. 2 and in Table 1, temperature is measured by RTD PT100 sensors, relative humidity by capacitive sensors and pressure by piezoelectric transmitters.

Volumetric flow rates are set by variable speed fans and are measured across an orifice plate. Each air stream flows in two different parallel ducts and pressure drop is measured across the orifice plate. Each duct can be excluded in case of low volumetric air flow tests to limit measurement uncertainty. Orifice plates and ducts apparatus are constructed according to DIN EN ISO 5167-2 standards [20]. Maximum supply air flow rate is 2000 $m^3\,h^{-1}$ while maximum exhaust air flow rate is 1400 $m^3\,h^{-1}$. Maximum volume flow rates achievable on the two air handling units are different since the experimental facility has been designed to test not only enthalpy but also desiccant wheels: in this case air flow across the wheel can be set unbalanced, which is quite a common condition especially at high regeneration temperatures.

Table 1
Sensors main data.

Abbreviation	Type of sensor	Accuracy*
$T1$**	PT 100 Class A	±0.2 °C
$T2$	PT 100 Class A	±0.2 °C
RH**	Capacitive	±1% (between 0 and 90%)
P	Piezoelectric	±0.5% of reading ±1 Pa

* At T = 20 °C.
** Temperature and relative humidity probe.

Fig. 1. Enthalpy wheels, tested in the present work, made of silica gel (*EW*1, left) and calcium carbonate (*EW*2, right) on aluminium substrate.

Enthalpy wheel revolution speed is controlled through an AC inverter motor in the range between 1 and 11 rev min^{-1}.

All calibrated sensors and actuators are connected to a National Instruments Compact Rio acquisition and control system, and controlled via Labview.

2.2. Experimental procedure

Each test is carried out in steady state conditions and in each session at least 300 samples of every physical quantity are registered (with a frequency of 1 Hz). Data are processed for outliers elimination and, subsequently, representative values for each working point are obtained as average of the remaining values.

At the end of each test the following quantities are calculated:

$$\dot{Q}_{S,sa} = \dot{m}_{sa} cp_{sa} \left(T_{sa,in} - T_{sa,out}\right) \tag{1}$$

$$\dot{Q}_{S,ea} = \dot{m}_{ea} cp_{ea} \left(T_{ea,out} - T_{ea,in}\right) \tag{2}$$

$$\dot{Q}_{L,sa} = \dot{m}_{sa} \lambda \left(X_{sa,in} - X_{sa,out}\right) \tag{3}$$

$$\dot{Q}_{L,ea} = \dot{m}_{ea} \lambda \left(X_{ea,out} - X_{ea,in}\right) \tag{4}$$

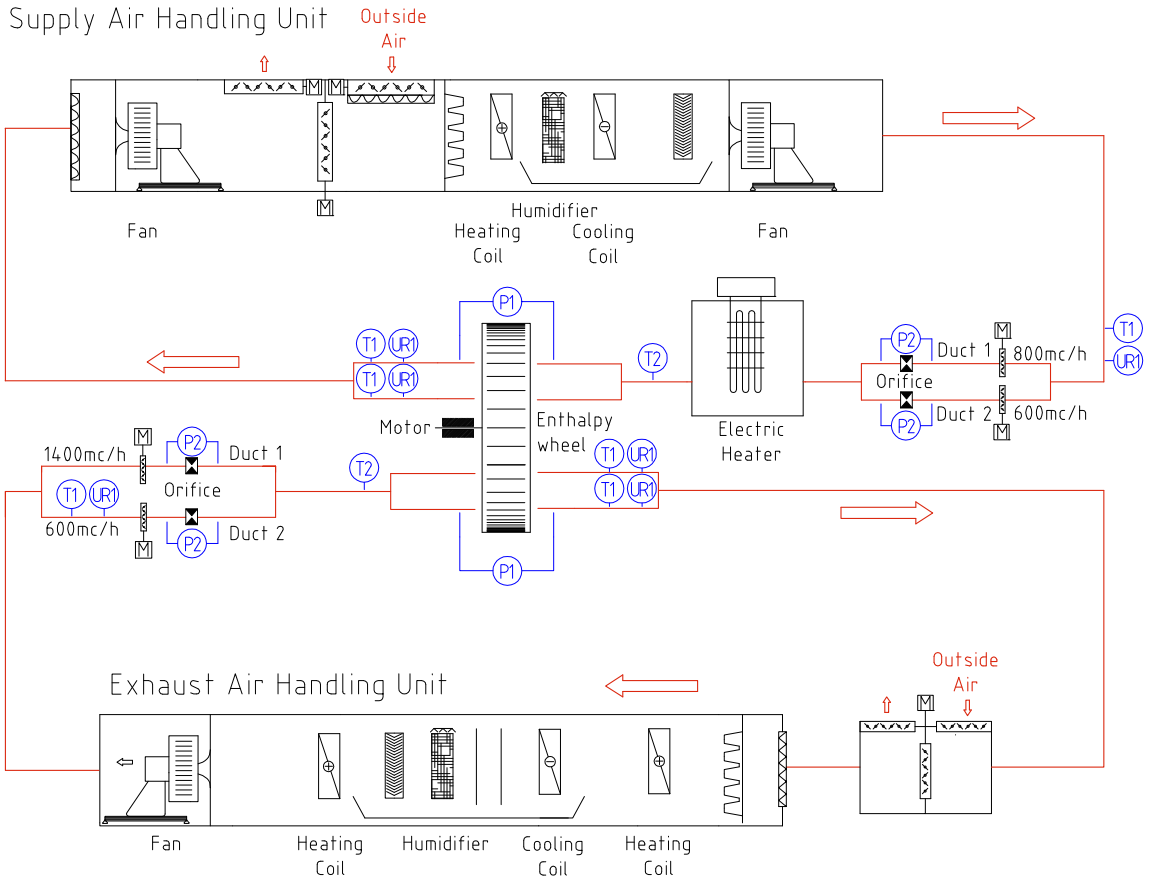

Fig. 2. Test rig scheme and instrumentation.

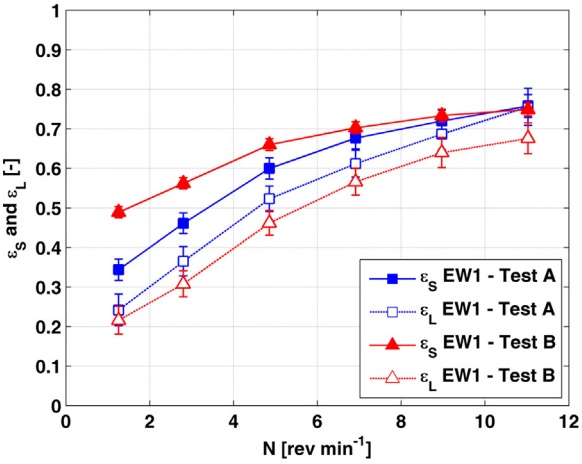

Fig. 3. *EW1*: Sensible and latent effectiveness against revolution speed.

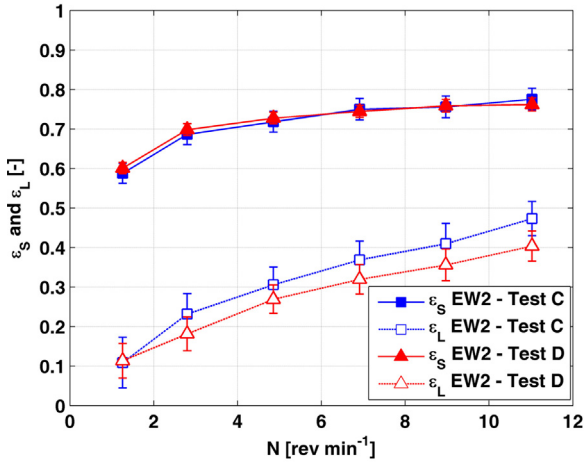

Fig. 4. *EW2*: Sensible and latent effectiveness against revolution speed.

Performance of each enthalpy wheel is determined through sensible and latent effectiveness, defined as:

$$\varepsilon_S = \frac{\left(\dot{Q}_{S,sa} + \dot{Q}_{S,ea}\right)/2}{\dot{Q}_{S,\max}} = \frac{\left(\dot{m}_{sa} cp_{sa}\left(T_{sa,in} - T_{sa,out}\right) + \dot{m}_{ea} cp_{ea}\left(T_{ea,out} - T_{ea,in}\right)\right)}{2(\dot{m}cp)_{\min}\left(T_{sa,in} - T_{ea,in}\right)} \quad (5)$$

and:

$$\varepsilon_L = \frac{\left(\dot{Q}_{L,sa} + \dot{Q}_{L,ea}\right)/2}{\dot{Q}_{L,\max}} = \frac{\left(\dot{m}_{sa}\lambda\left(X_{sa,in} - X_{sa,out}\right) + \dot{m}_{ea}\lambda\left(X_{ea,out} - X_{ea,in}\right)\right)}{2(\dot{m}\lambda)_{\min}\left(X_{sa,in} - X_{ea,in}\right)} \quad (6)$$

where $T_{sa,out}$, $T_{ea,out}$, $X_{sa,out}$ and $X_{ea,out}$ are the average values of temperature and humidity ratio based on the physical quantities collected by the two sensors installed, respectively, at the supply air stream outlet and at the exhaust air stream outlet. While the temperature is directly measured, the humidity ratio is calculated from the measured values of temperature and relative humidity in the following way:

$$X_a = 0.622\frac{p_{vsat}\,\varphi_a}{p_{tot,a} - p_{vsat}\,\varphi_a} \quad (7)$$

where $p_{tot,a}$ is the atmospheric air pressure, assumed constant and equal to 101,325 Pa, φ_a is the air relative humidity and p_{vsat} is the water vapour saturation pressure calculated with the following correlation:

$$p_{vsat} = e^{23.196 - \left(3816.44/(T_a + 273.13) - 46.13\right)} \quad (8)$$

The water latent heat of vaporization λ is assumed constant and equal to 2501×10^3 J kg^{-1}.

The mass flow rate of each air stream is calculated through appropriate correlations involving temperature, relative humidity and pressure drop across each orifice plate installed in the ducts [20]. Therefore it is $\dot{m}_{sa} = \dot{m}_{sa}\left(T_{sa,op}, \varphi_{sa,op}, \Delta p_{sa,op,D1}, \Delta p_{sa,op,D2}\right)$ and $\dot{m}_{ea} = \dot{m}_{ea}\left(T_{ea,op}, \varphi_{ea,op}, \Delta p_{ea,op,D1}, \Delta p_{ea,op,D2}\right)$.

The uncertainty of both calculated effectiveness, reported from Figs. 3–6, is estimated in accordance with the law of propagation of error [21,22]. Therefore sensible and latent effectiveness are both function of several measured quantities x_i, namely: $T_{sa,in}$, $\varphi_{sa,in}$, $T_{sa,out}$, $\varphi_{sa,out}$, $T_{ea,in}$, $\varphi_{ea,in}$, $T_{ea,out}$, $\varphi_{ea,out}$, $T_{sa,op}$, $\varphi_{sa,op}$, $\Delta p_{sa,op,D1}$, $\Delta p_{sa,op,D2}$, $T_{ea,op}$, $\varphi_{ea,op}$, $\Delta p_{ea,op,D1}$ and $\Delta p_{ea,op,D2}$.

The experimental uncertainty u_{xi} of each monitored variable x_i is:

$$u_{x_i} = \pm\sqrt{u_{x_{i,inst}}^2 + \left(t_{95}\,\sigma_{\bar{x}_i}\right)^2} \quad (9)$$

where $u_{xi,inst}$ is the instrument uncertainty of the generic measured parameter, t_{95} is the student test multiplier at 95% confidence and $\sigma_{\bar{x}_i}$ is the standard deviation of the mean.

The combined uncertainty of sensible or latent effectiveness u_ε is calculated as:

$$u_\varepsilon = \sqrt{\sum_i \left(\frac{\partial \varepsilon}{\partial x_i} u_{x_i,inst}\right)^2 + t_{95}^2 \sum_i \left(\frac{\partial \varepsilon}{\partial x_i}\sigma_{\bar{x}_i}\right)^2} \quad (10)$$

Pressure drop has been measured through a specific test performed for each enthalpy wheel. Also in this case, after outliers elimination, pressure drop of each working point has been calculated as the average of the measured values and its uncertainty through Eq. (9).

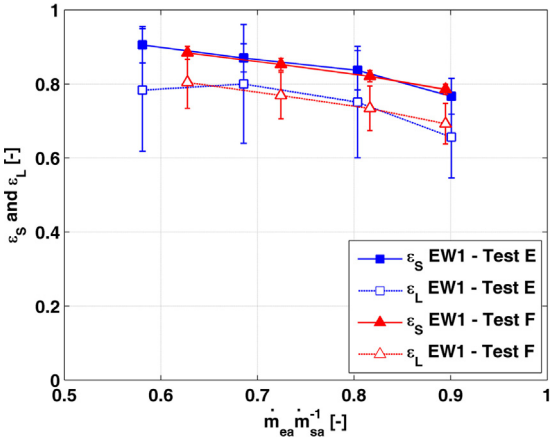

Fig. 5. *EW1*: Sensible and latent effectiveness against exhaust air to supply air mass flow ratio.

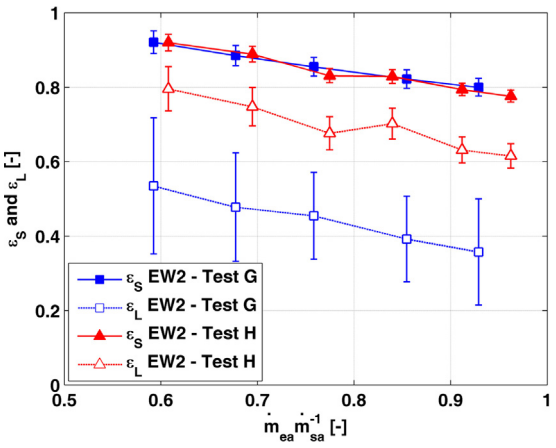

Fig. 6. *EW*2: Sensible and latent effectiveness against exhaust air to supply air mass flow ratio.

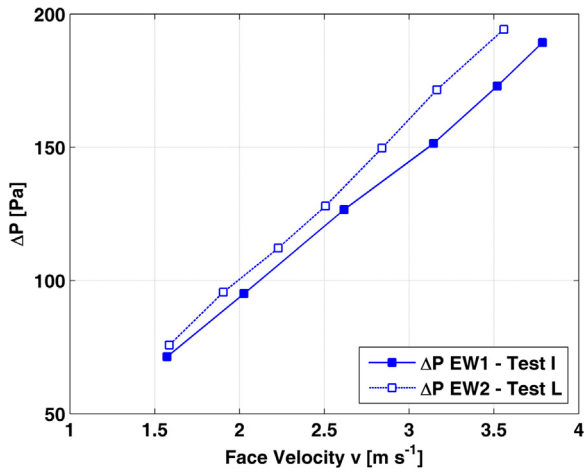

Fig. 7. *EW*1 and *EW*2: pressure drop against face air velocity.

3. Experimental performance

3.1. Enthalpy wheel description and tests arrangement

In this work two different enthalpy wheels, denoted, respectively, with *EW*1 and *EW*2, are tested. They are both made of aluminium coated with an adsorbent material: silica gel for *EW*1 and calcium carbonate for *EW*2. Cross section area of both wheels is divided in two equal parts: the former for the supply air stream and the latter for exhaust air stream. In both cases no purge sector is adopted. Main features of *EW*1 and *EW*2 are provided in Table 2.

Several tests have been performed in different working conditions, in particular varying inlet air temperature, humidity and the flow rate of each stream, as reported in Table 3. It is pointed out that in all tests there is no vapour condensation or frost formation along enthalpy wheels channels.

3.2. Sensible and latent effectiveness

In Figs. 3 and 4 sensible and latent effectiveness of, respectively, *EW*1 and *EW*2 are reported, as a function of the revolution speed. All the tests are performed with balanced flows and air face velocity around 2.4 m s^{-1}. Some preliminary considerations can be outlined:

- The higher the revolution speed, the higher the sensible and latent effectiveness and the higher the air stream mixing due to a larger amount of air trapped in the wheel channels. Effectiveness curve slope is particularly sharp at low revolution speed and becomes almost flat when N is higher than 10 rev min^{-1}, as clearly confirmed in literature [7,9,23]. Therefore the optimal revolution speed should be higher than 10 rev min^{-1} and, at the same time, as low as possible to reduce air mixing. In this work it is assumed an optimal revolution speed $N = 11$ rev min^{-1}, corresponding to an air mixing of around 2% with a face velocity of 2.4 m s^{-1}.
- In correspondence of $N = 11$ rev min^{-1}, sensible effectiveness of *EW*1 and of *EW*2 are almost equal ($\varepsilon_S \approx 0.78$). This result is consistent with the fact that enthalpy wheels are made of the same supporting material, with similar geometry and heat capacity. In these working conditions sensible effectiveness is almost independent of inlet air stream temperatures.
- Latent effectiveness increases with revolution speed as described for the sensible effectiveness. Latent effectiveness of *EW*1 is much higher than the one of *EW*2, mostly due to the higher quantity of adsorbent materials and its different properties.
- At nominal rotational speed $N = 11$ rev min^{-1}, depending on test conditions, latent effectiveness of *EW*1 is between 0.68 and 0.78 while the one of *EW*2 is between 0.40 and 0.60.

In Figs. 5 and 6 sensible and latent effectiveness of both enthalpy wheels are reported for unbalanced air flows. When the face velocity of one of the air stream decreases, effectiveness increases because the ratio between the heat exchanger area and the air flow becomes higher. This effect should be properly taken into account in real applications, where the exhaust air stream can be lower than the supply air one, in order to keep a slightly higher pressure in the building and minimize air infiltration through the envelope. It is possible to state that the lower the face velocity, the higher the effectiveness of the heat exchanger. Instead the lowest value of effectiveness is reached in case of balanced air flows and high face velocity. Typically air velocity at enthalpy wheel face is around 2.5 m s^{-1}, with minimum and maximum values in the range between 1.5 and 3.5 m s^{-1}. Lower values would lead to extremely large device size, while higher velocities would bring about poor performance and detrimental pressure drops.

It should be put in evidence that sensible effectiveness is almost independent of air temperature and humidity while latent effectiveness is influenced by inlet air conditions. In fact in this case performance depends on air conditions because vapour adsorption and desorption process is related to air temperature and humidity profile across the wheel channels. In particular the slope of the adsorption isotherm influences the water vapour mass transfer between the air streams and the wheel matrix. At nominal revolution speed and balanced air flows, the latent effectiveness of *EW*1 varies slightly with inlet air conditions, probably due to the adsorption isotherm slope of silica gel that can be assumed almost constant in a wide range of relative humidity and temperature. Instead, the latent effectiveness of *EW*2 turns out to depend on inlet conditions: this behaviour may be induced by the particular adsorption isotherm slope of the *EW*2 coating, which is unknown and has not been investigated in the present work. In particular, as reported in results of test *H* of *EW*2, it is shown that the lower the air average temperature, the higher the latent effectiveness.

3.3. Pressure drop

In Fig. 7 pressure drop is reported as a function of face air velocity. In both *EW*1 and *EW*2 pressure drop is almost linear with the air flow, as laminar pressure drops across the channel are dominant compared to local pressure loss due to channel entrance (enthalpy

Table 2
Enthalpy wheels technical data.

Enthalpy wheel	Matrix material	Adsorption material	a_c [mm]	b_c [mm]	$D_{EW,o}$ [m]	$D_{EW,h}$ [m]	L [m]	$A_{EW,sa}$ or $A_{EW,ea}$ [m^2]	Purge sector
*EW*1	Aluminum	Silica gel	1.7	3.2	0.6	0.08	0.2	0.1388	None
*EW*2	Aluminum	Calcium carbonate	1.7	3.2	0.6	0.08	0.2	0.1388	None

Table 3
Tests conditions.

Test	Enthalpy Wheel	$\dot{m}_{ea}$ [kg s^{-1}]	$T_{ea,in}$ [°C]	$X_{ea,in}$ [g kg^{-1}]	$\dot{m}_{sa}$ [kg s^{-1}]	$T_{sa,in}$ [°C]	$X_{ea,in}$ [g kg^{-1}]	N [rev min^{-1}]
A	*EW*1	0.413	24.0	8.7	0.405	29.6	14.4	1–11
B	*EW*1	0.412	26.0	9.8	0.394	36.8	17.8	1–11
C	*EW*2	0.419	23.9	9.4	0.407	29.8	13.7	1–11
D	*EW*2	0.418	26.1	10.8	0.408	36.8	18.2	1–11
E	*EW*1	0.241–0.410	25.8	10.7	0.411	30.1	12.4	11
F	*EW*1	0.232–0.393	25.4	11.9	0.352	37.7	17.3	11
G	*EW*2	0.240–0.411	25.6	10.5	0.404	33.0	12.5	11
H	*EW*2	0.252–0.412	14.2	6.7	0.423	24.4	10.9	11
I	*EW*1	0.235–0.416	10.0–23.0	5.0–12.0	0.239–0.401	25.0–33.7	12.0–15.0	11
L	*EW*2	0.241–0.408	13.2–20.1	6.0–11.0	0.233–0.421	22.0–41.4	10.9–24.2	11
M	*EW*1	0.182–0.428	19.6	5.4	–	–	–	11
N	*EW*2	0.185–0.444	20.0	5.5	–	–	–	11

wheel inlet section) and sudden expansion (outlet section). Test conditions are summarized in Table 3.

4. Practical correlations

4.1. Common considerations

In relation to the experimental results reported above, practical correlations to predict sensible effectiveness, latent effectiveness and pressure drop have been developed.

Both effectiveness correlations are expressed as a function of face velocity instead of air mass flow rate. In this way the equations can be easily adapted for heat exchangers of different diameters. Correlations are developed at reference wheel revolution speed of $N = 11$ rev min^{-1}. Effects of different rotational speed are not taken into account because of limited interest in HVAC applications. Sensible and latent effectiveness are based on tests from *A* to *L* (neglecting cases with $N < 11$ rev min^{-1}) and pressure drop correlations are determined from test *M* and *N* (Table 3).

All the coefficients C and exponents n used in the correlations are summarized in Table 4 for both enthalpy wheels. They have been calculated through an appropriate numeric tool, minimizing the root mean squared deviation between the correlation results and the actual values based on measurements.

4.2. Sensible effectiveness correlation

Sensible effectiveness correlations have been developed adopting the formulation proposed by Kays and London [16], properly modified in order to be function of inlet air velocity instead of the air flow rate. In particular the original formula has been modified assuming constant specific heat of wet air and, therefore, considering that $NTU = UA/(\dot{m}\,cp)_{min} = C/(v_{a,in}\,\rho_{a,in})_{min}$, where C is the generic correlation parameter.

In this work equation parameters are not directly calculated from actual wheel data but they are determined by performing a fitting on experimental tests (50 tests for *EW*1 and 43 tests for *EW*2), as already reported in Section 4.1. According to [16], sensible effectiveness is calculated as follows:

$$\varepsilon_S = \varepsilon_{S,0}\,\alpha_S \tag{11}$$

where:

$$\varepsilon_{S,0} = \frac{1 - e^{(C_1/(v_{a,in}\rho_{a,in})_{\min})(R-1)}}{1 - R\,e^{(C_1/(v_{a,in}\rho_{a,in})_{\min})(R-1)}} \tag{12}$$

$$\alpha_S = 1 - \frac{1}{C_2\left(C_3/(v_{a,in}\rho_{a,in})_{min}\right)^{n_1}} \tag{13}$$

where R is the ratio between the minimum and maximum values of inlet air velocity times inlet air density:

$$R = \frac{(\dot{m}\ cp)_{\min}}{(\dot{m}\,cp)_{\max}} = \frac{\left(v_{a,in}\ A\rho_{a,in}\ cp\right)_{\min}}{\left(v_{a,in}\ A\rho_{a,in}\ cp\right)_{\max}} = \frac{\left(v_{a,in}\ \rho_{a,in}\right)_{\min}}{\left(v_{a,in}\ \rho_{a,in}\right)_{\max}} = \frac{\min\left(v_{sa,in}\ \rho_{sa,in};\ \ v_{ea,in}\ \rho_{ea,in}\right)}{max\left(v_{sa,in}\ \rho_{sa,in};\ \ v_{ea,in}\ \rho_{ea,in}\right)} \tag{14}$$

Calculated and experimental sensible effectiveness are reported in Fig. 8. Relative errors between predicted and measured values of

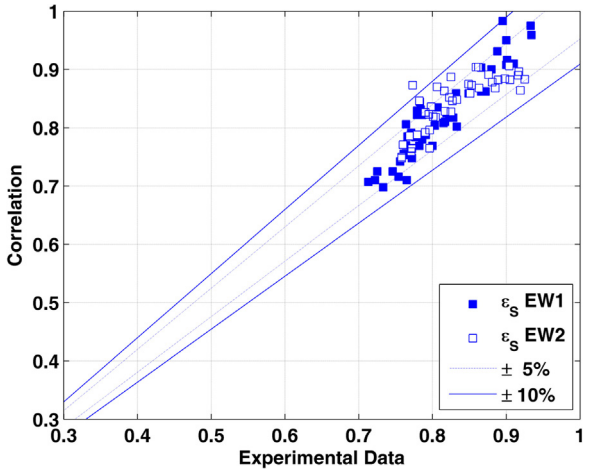

Fig. 8. *EW*1 and *EW*2: Calculated and experimental sensible effectiveness.

Table 4
Parameters used in the correlations.

Enthalpy wheel	Sensible effectiveness				Latent effectiveness							Pressure drop	
	C_1	C_2	C_3	n_1	C_4	C_5	C_6	n_2	C_7	C_8	n_3	C_9	C_{10}
*EW*1	7.133	8.45	8.34	9	5.476	9	7.626	1.93	0	1	0	219000	1.93
*EW*2	40.528	8.138	1.998	1.15	7.36	4.15	0.759	0.65	0.22	1/28	−3.82	221000	2.86

Table 5
Reference high and low values of test conditions used to determine the correlations.

Sensible and latent effectiveness								Pressure Drop
Enthalpy wheel	$v_{ea,in}$ [m s^{-1}]	$T_{ea,in}$ [°C]	$X_{ea,in}$ [g kg^{-1}]	$v_{sa,in}$ [m s^{-1}]	$T_{sa,in}$ [°C]	$X_{ea,in}$ [g kg^{-1}]	N [rev min^{-1}]	$v_{a,in}$ [m s^{-1}]
*EW*1	1.2–2.5	10.0–26.0	5.0–12.0	1.2–2.5	25.0–37.7	12.0–17.8	11	1.6–3.8
*EW*2	1.2–2.5	13.2–26.1	6.0–11.0	1.2–2.5	22.0–41.4	10.9–24.2	11	1.6–3.8

*EW*1 and *EW*2 are within ±10%, respectively, in 100% and in 97.7% of the analyzed cases.

Both proposed correlations are valid in the range reported in Table 5. Anyway, as shown in Section 3.2, they are expected to work properly also in a wider range of working conditions typical of HVAC systems, such as during winter time characterized by a lower supply air temperature.

4.3. Latent effectiveness correlation

Latent effectiveness correlation has the same formulation of the sensible one, except for an additional term β_L. In this case correlation parameters are calculated by fitting 50 experimental data for *EW*1 and 35 for *EW*2, minimizing the root mean square deviation. The latent effectiveness is:

$$\varepsilon_L = \varepsilon_{L,0}\,\alpha_L\,\beta_L \tag{15}$$

where:

$$\varepsilon_{L,0} = \frac{1 - e^{(C_4/(v_{a,in}\,\rho_{a,in})_{\min})(R-1)}}{1 - R\,e^{(C_4/(v_{a,in}\,\rho_{a,in})_{\min})(R-1)}} \tag{16}$$

$$\alpha_L = 1 - \frac{1}{C_5\left(C_6/\left(v_{a,in}\,\rho_{a,in}\right)_{\min}\right)^{n_2}} \tag{17}$$

An additional term β_L is added in order to take into account the effect of inlet air conditions on the latent effectiveness, as previously explained in Section 3.2. Simonson and Besant [18] proposed a complex correlation that depends on many parameters, such as *NTU*, air temperature, relative humidity, revolution speed, matrix thermal capacity, adsorption isotherm slope and maximum sensible and latent exchangeable heat. The term β_L proposed in this work is a simplified form of the aforementioned correlation including only the dependence on the average temperature:

$$\beta_L = 1 + C_7(C_8\,T_{ave})^{n_3} \tag{18}$$

Where the average temperature is:

$$T_{ave} = \frac{\dot{m}_{sa}\;cp_{sa}\,T_{sa,in} + \dot{m}_{ea}\;cp_{ea}\,T_{ea,in}}{\dot{m}_{sa}\;cp_{sa} + \dot{m}_{ea}\;cp_{ea}} \tag{19}$$

According to experimental data analysis, the dependence of the latent effectiveness on humidity has been neglected for both enthalpy wheels and the dependence of latent effectiveness on temperature has been neglected only for *EW*1. It should be put in evidence that:

- If the term β_L is introduced in the latent effectiveness correlation of *EW*1 and appropriate coefficients and exponents are evaluated, the root mean square deviation decreases only by 1%. Therefore in this case the term β_L has not been adopted.
- If the term β_L is not used in the evaluation of the latent effectiveness correlation of *EW*2, the root mean square deviation increases by 40%.
- The use of an additional term taking into account the effect of average humidity has been evaluated, carrying out to an insignificant reduction of the root mean square deviation.

Comparison between calculated and experimental latent effectiveness is shown in Fig. 9. Relative errors are within ±10%, respectively, in 83.7% and 61.2% of the analyzed cases of *EW*1 and *EW*2.

Validity ranges of latent effectiveness are reported in Table 5. While the correlation of *EW*1 is reasonably valid slightly outside this range, the correlation of *EW*2 is strongly influenced by the term β_L, which depends on the wheel average temperature. In particular attention should be paid if T_{ave} is lower than 16.5 °C. In order to avoid wrong calculation, if the product $\alpha_L\;\beta_L$ is higher than 1 it should be assumed equal to 1, and it becomes $\varepsilon_L = \varepsilon_{L,0}$.

4.4. Pressure drop correlation

Distributed and local pressure drop across the enthalpy wheel are evaluated in the following way:

$$\Delta p_d = C_9\,v_{a,in}\,\rho_{a,in} v_{a,in} \tag{20}$$

$$\Delta p_l = C_{10}\,\rho_{a,in} v_{a,in}^2 \tag{21}$$

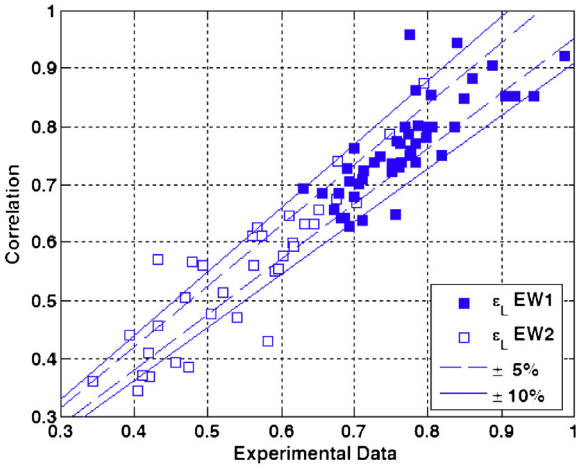

Fig. 9. *EW*1 and *EW*2: Calculated and experimental latent effectiveness.

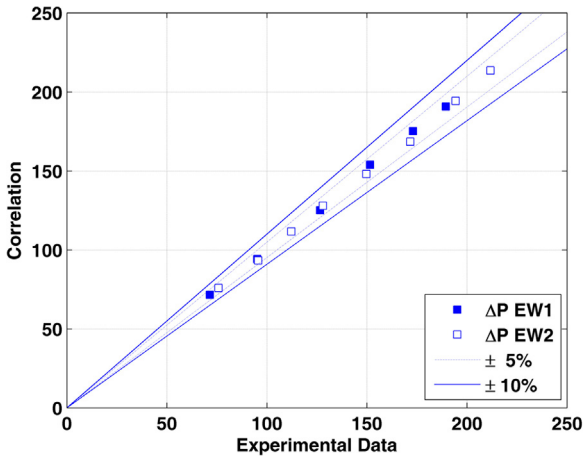

Fig. 10. *EW*1 and *EW*2: Calculated and experimental pressure drop.

The total pressure drop is therefore:

$$\Delta p_{tot} = \Delta p_d + \Delta p_l \tag{22}$$

The coefficients C_9 and C_{10}, reported in Table 4, have been determined fitting experimental data and considering during tests of both wheels an average density $\rho_{a,in} = 1.2\,\mathrm{kg\,m^{-3}}$ and an average cinematic viscosity $\nu_{a,in} = 16 \times 10^{-5}\,\mathrm{m^2\,s^{-1}}$.

In Fig. 10 comparison between calculated and experimental data is shown. For *EW*1 the relative difference is always within ±1.6% and for *EW*2 it is within ±2.5%.

5. Conclusions

In this work two different enthalpy wheels have been tested and main experimental results are reported with calculated level of uncertainty. Both rotary heat exchangers are made of aluminium coated with an adsorbent material: silica gel in the first case and calcium carbonate in the second one. Both wheels show similar sensible effectiveness and pressure drop, but the silica gel based device appears to be more effective for latent heat recovery.

Practical correlations to predict sensible effectiveness, latent effectiveness and pressure drop are developed for both enthalpy wheels. These correlations are able to predict the performance of the two rotary heat exchangers properly and owing to their simple formulation, they might be particularly suitable for energy simulation tools for building—HVAC systems.

Acknowledgments

Funding for this work from Italian Cassa Conguaglio Sistema Elettrico under agreement no. 6562 is acknowledged (project STAR— Sidera Trigenerazione Alto Rendimento). The authors would like to thank Mr Leone, Mr Bawa and Mr Liberati of Recuperator S.p.A. for the information provided.

References

[1] A. Mardiana, S.B. Riffat, Review on physical and performance parameters of heat recovery systems for building applications, Renewable and Sustainable Energy Reviews 28 (2013) 174–190.
[2] M. Rasouli, C.J. Simonson, R.W. Besant, Applicability and optimum control strategy of energy recovery ventilators in different climatic conditions, Energy and Buildings 42 (2010) 1376–1385.
[3] C.E.L. Nóbrega, N.C.L. Brum, An analysis of the heat and mass transfer roles in air dehumidification by solid desiccants, Energy and Buildings 50 (2012) 251–258.
[4] TRNSYS, TRNSYS 16—A Transient System Simulation Program, Solar Energy Laboratory, University of Wisconsin–Madison, Madison, WI, 2005.
[5] DOE, Energy Plus Engineering Reference, The Reference to Energy Plus Calculations, DOE, US, 2013.
[6] Z. Wu, R.V. Melnik, F. Borup, Model-based analysis and simulation of regenerative heat wheel, Energy and Buildings 38 (2006) 502–514.
[7] L.Z. Zhang, J.L. Niu, Performance comparisons of desiccant wheels for air dehumidification and enthalpy recovery, Applied Thermal Engineering 22 (2002) 1347–1367.
[8] C.J. Simonson, R.W. Besant, Energy wheel effectiveness: Part I—Development of dimensionless groups, International Journal of Heat and Mass Transfer 42 (1999) 2161–2170.
[9] R. Tu, X.H. Liu, Y. Jiang, Performance comparison between enthalpy recovery wheels and dehumidification wheels, International Journal of Refrigeration 36 (2013) 2308–2322.
[10] C.E.L. Nóbrega, N.C.L. Brum, Modeling and simulation of heat and enthalpy recovery wheels, Energy 34 (2009) 2063–2068.
[11] L.A. Sphaier, W.M. Worek, Parametric analysis of heat and mass transfer regenerators using a generalized effectiveness-NTU method, International Journal of Heat and Mass Transfer 52 (2009) 2265–2272.
[12] C.R. Ruivo, J.J. Costa, A.R. Figueiredo, Analysis of simplifying assumptions for the numerical modeling of the heat and mass transfer in a porous desiccant medium, Numerical Heat Transfer Applications 49 (2006) 851–872.
[13] C.R. Ruivo, J.J. Costa, A.R. Figueiredo, On the validity of lumped capacitance approaches for the numerical prediction of heat and mass transfer in desiccant airflow systems, International Journal of Thermal Sciences 47 (2008) 282–292.
[14] D.Y. Lee, D.S. Kim, Analytical modeling of a desiccant wheel, International Journal of Refrigeration 42 (2014) 97–111.
[15] A.A. Rabah, A. Fekete, S. Kabelac, Experimental investigation on a rotary regenerator operating at low temperatures, Journal of Thermal Science and Engineering Applications 1 (2009) 0410041–0410049.
[16] W. Kays, A.L. London, Compact Heat Exchangers, Mc Graw Hill, New York, NY, 1984.
[17] G. Stiesch, Performance of rotary enthalpy exchangers, in: Doctoral Dissertation, University of Wisconsin, Wisconsin, 1994.
[18] C.J. Simonson, R.W. Besant, Energy wheel effectiveness: Part II—Correlations, International Journal of Heat and Mass Transfer 42 (1999) 2171–2185.
[19] J.W. Jeong, S.A. Mumma, Practical thermal performance correlations for molecular sieve and silica gel loaded enthalpy wheels, Applied Thermal Engineering 25 (2005) 719–740.
[20] DIN EN ISO 5167-2 Standards, Measurement of fluid flow by means of pressure differential devices inserted in circular cross-section conduits running full—Part 2: Orifice plates (ISO 5167-2:2003), 2003.
[21] ISO IEC Guide 98-3, Uncertainty of Measurement—Part 3: Guide to Expression of Uncertainty in Measurement, International Organization for Standardization, ISO IEC Guide 98-3, Geneva Switzerland, 2008.
[22] R.J. Moffat, Describing the uncertainties in experimental results, Experimental Thermal and Fluid Science 1 (1988) 3–10.
[23] N. Enteria, H. Yoshino, A. Satake, A. Mochida, R. Takaki, R. Yoshie, T. Mitamura, S. Baba, Experimental heat and mass transfer of the separated and coupled rotating desiccant wheel and heat wheel, Experimental Thermal and Fluid Science 34 (2010) 603–615.